

RSC Advances



This is an *Accepted Manuscript*, which has been through the Royal Society of Chemistry peer review process and has been accepted for publication.

Accepted Manuscripts are published online shortly after acceptance, before technical editing, formatting and proof reading. Using this free service, authors can make their results available to the community, in citable form, before we publish the edited article. This *Accepted Manuscript* will be replaced by the edited, formatted and paginated article as soon as this is available.

You can find more information about *Accepted Manuscripts* in the [Information for Authors](#).

Please note that technical editing may introduce minor changes to the text and/or graphics, which may alter content. The journal's standard [Terms & Conditions](#) and the [Ethical guidelines](#) still apply. In no event shall the Royal Society of Chemistry be held responsible for any errors or omissions in this *Accepted Manuscript* or any consequences arising from the use of any information it contains.



Journal Name

ARTICLE

Easy Access to Nitrogen-Doped Mesoporous Interlinked Carbon/NiO Nanosheet for application in lithium-ion batteries and supercapacitors

Received 00th January 20xx,
Accepted 00th January 20xx

DOI: 10.1039/x0xx00000x

www.rsc.org/

Yuan Xia,^a Beibei Wang,^a Gang Wang,^b and Hui Wang^{a,*}

We report a simple route to synthesis nitrogen-doped mesoporous interlinked carbon/NiO nanosheet that consist of carbon nanosheets and monodisperse NiO nanoparticles embedded in them homogeneously. The nitrogen-doped mesoporous interlinked carbon/NiO nanosheet with carbon content of 46% was obtained through directly low temperature heat treatment of Ni-ZIF-8 with a rapid heating rate (5 °C min⁻¹). During the heat treatment, a large number of mesoporous were formed in the product with the evaporation (or thermal decomposition) of the organic ligand. When tested as an anode for lithium ion batteries (LIBs), the unique structure of the mesoporous carbon/NiO nanosheet not only shortened electro- and iron-transport path-ways but also accommodated the volume change during Li⁺ intercalation and deintercalation process, resulting in a reversible capacity of 627 mAh g⁻¹ at 0.5 A g⁻¹ after 300 cycles. Moreover, the as-assembled carbon/NiO nanosheet supercapacitor can also exhibit an excellent cycling performance (414 F g⁻¹ at 5 A g⁻¹) with 92.2% specific capacitance retention after 3000 cycles by combined the pseudocapacitive behavior of the NiO nanoparticles with the electric double-layer capacitors (EDLCs) of the nitrogen-doped mesoporous carbon.

Introduction

Transition metal oxides (TMOs) are a well-known class of materials mainly used for catalysis, energy storage and conversion due to their unique properties.¹⁻³ In the last few years with continuous development of synthetic technique, which allow accessing these materials with low-cost under the conditions of eco-friendly, the interest toward those materials has been greatly increased, especially in the field of energy storage, such as lithium ion battery and supercapacitor.^{4,5} However, there are still several challenges associated with the TMO electrode materials for using in lithium store or electronic reserves, such as volume change, poor electronic and ionic conductivity, and severe aggregation.⁶⁻⁸ To address those problems, many efforts have been devoted to obtain various TMOs with porous or nano- structures, which can significantly influence their cycling stability and long cycle lifetime.⁹⁻¹¹ Of these methods, carbon-modified, which included carbon-coated¹²⁻¹⁴ and carbon-supported,^{15,16} is recognized as a very effective and commonly used way for improving the electronic conductivity and thus the electrochemical performance of TMOs. The conventional carbon-supported approach involves the use of

some expensive carbon materials, like carbon cloth,¹⁶ graphene¹⁷ or carbon nanotube¹⁸. And the formation of carbon-coated TMOs were mainly performed via a pyrolysis of sugar or polymer,¹⁹⁻²¹ or a chemical vapor deposition method.^{22,23} Unavoidably, both of the two methods eventually need a high temperature treatment process.

Metal-organic frameworks (MOFs) synthesized by assembling metal ions with organic ligands are a new class of hybrid nanoporous materials.²⁴⁻²⁶ It can be considered as effective sacrificial templates or precursors to synthesis porous metal oxide.^{27,28} After annealing, the metal ions in the MOFs can be converted to metal oxides, and the organic ligands are carbonized to form mesoporous carbon, which inherits the porous morphology to the nanoscale MOF precursors. As modified materials, the mesoporous carbon material combines the advantages of many kinds of materials, such as large specific surface, high porosity, and abundant active site.^{29,30} The composites with mesoporous carbon as their template or support can effectively enhance the property of the materials and make the materials possess various functions. In addition, if the organic ligands contain heteroatoms, the corresponding mesoporous carbon material would be modified by atomic or molecular. Doping elements in carbon materials,³¹⁻³⁴ such as phosphorus, boron and nitrogen elements, can significantly improve the electrochemical performance by changing the form of carbon's hybrid orbit. Among numerous doping elements, N-doped can change the distribution of electrostatic potential and strengthen the electric effect of its surrounding system.³⁵ This is for the reason that the nitrogen atom can influence its surrounding carbon atoms to establish a positive electrostatic potential area (PEPA). However, without the doping elements, the electrostatic

^aKey Laboratory of Synthetic and Natural Functional Molecule Chemistry (Ministry of Education), College of Chemistry & Materials Science, Northwest University, Xi'an 710069, PR China, E-mail address: huiwang@nwu.edu.cn (H. Wang).

^bNational Key Laboratory of Photoelectric Technology and Functional Materials (Culture Base), National Photoelectric Technology and Functional Materials & Application International Cooperation Base, Institute of Photonics & Photon-Technology, Northwest University, Xi'an 710069, PR China.

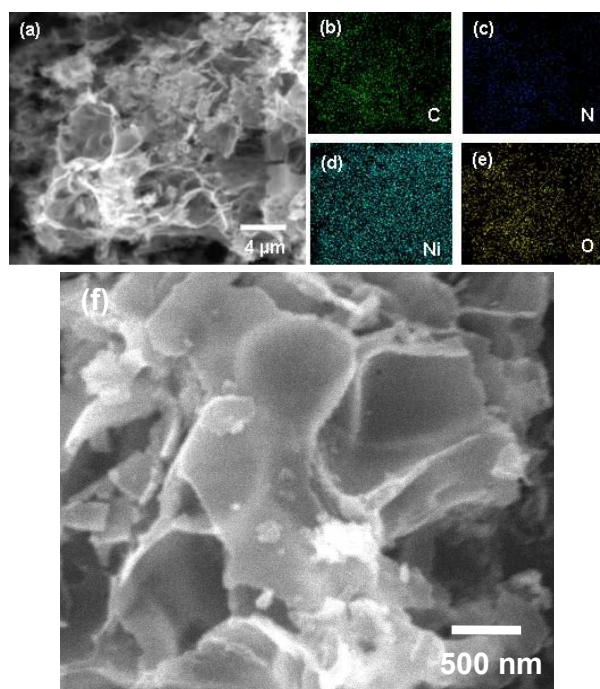


Fig. 1 SEM and corresponding EDX-mapping images of carbon/NiO nanosheet.

potential of carbon materials will be uniformly distributed on each carbon atom. Just because of the existence of the PEPA, donated electronic abilities and electrical conductivity of the materials are enhanced and the electrochemical active sites are increased. All of the above principles are very helpful to the storage of lithium ion or to the usage for supercapacitor.³⁶

A new nanocomposite with a much larger application space and a greater developmental potential will be produced if nanosize TMOs are combined with nitrogen-doped mesoporous carbon materials. In this study, we report on a novel nitrogen-doped mesoporous interlinked carbon/NiO nanosheet fabricated using Ni-MOF-8 as both the precursor and the self-sacrificing template. The synthesis route includes a precipitation reaction to form MOFs at room temperature and a subsequently thermal treatment process at 350 °C in the argon protection. Our strategy is simple in operation and low in cost, and most important it is very applicable to large-scale production with good controllability. In the synthesized carbon/NiO nanosheet product, monodispersed NiO nanoparticles with an average particle size of around 10 nm are uniformly dispersed and embedded in mesoporous carbon. When evaluated as electrode materials, the as-prepared carbon/NiO nanosheet can exhibit high lithium storage capacity and excellent supercapacitive performance

Experimental

Synthesis of Nanocomposite

All reagents are of analytical reagent grade and used without further purification. Ni-ZIF-8 was synthesized through a modified method according to the literature.³⁷ Typically, 780 mg

Ni(NO₃)₂·6H₂O was dissolved in 20 mL of ethanol, then quickly poured into 20 mL methanol solution of 2-methylimidazole. After ageing overnight at room temperature, the green crystalline precipitate of Ni-ZIF-8 was obtained by filter. In order to obtain nitrogen-doped mesoporous interlinked carbon/NiO nanosheets (C/NiO nanosheets), the precipitate Ni-ZIF-8 was annealed at 350 °C for 30 min with a rapid heating rate of 5 °C min⁻¹ in the argon protection and then naturally cooled to room temperature in air atmosphere.

Material Characterization

The powder X-ray (XRD) diffraction pattern was measured using a Bruker D8 ADVANCE diffractometer with high-intensity Cu K α irradiation ($\lambda = 1.5406 \text{ \AA}$). The morphology of the products was examined by Field-emission scanning electron microscopy (FESEM, JEOL JSM-6390A) and high-resolution transmission electron microscopy (HRTEM, JEOL JEM-2100). X-ray photoelectron spectroscopy (XPS) measurements were collected using a PHI-5400 electron spectrometer equipped with an Al anode (Al K $\alpha = 1846.6 \text{ eV}$). Thermogravimetric analysis (TGA) was performed with a STA 449C thermobalance with a temperature ramp of 10 °C min⁻¹. Nitrogen adsorption/desorption measurements (BET measurement) were performed on a Tristar II3020 N₂ absorption equipment at 77 K.

Lithium Ion Battery Measurement

The working electrodes were prepared by directly depressing the C/NiO nanosheet on Ni foam at 20 MPa. Lithium ion battery performance test were carried out using two-electrode coin cells by using microporous polypropylene film as the separator and pure lithium foils as counter electrodes. The electrolyte was a solution of 1 M LiPF₆ in a mixture of diethyl carbonate and ethylene carbonate at a 7:3 volume ratio. The charge and discharge tests were operated on a LAND battery program-control test system (CT 2001A) in the voltage range of 0.005–3.0 V (vs Li/Li⁺). Cyclic voltammetry (CV) was performed on electrochemical workstation (CHI 660D) at various scanning rates of 0.2 mV s⁻¹, respectively.

Supercapacitor Measurement

The electrochemical performance of supercapacitor was studied using a three-electrode test system with C/NiO nanosheet as the working electrode, platinum foil as the counter electrode, Ag/AgCl as the reference electrode, and 0.5 M K₂SO₄ aqueous solution as electrolyte. The working electrode was prepared by loading a slurry consisting of 80 wt % C/NiO nanosheet, 10 wt % acetylene black, and 10 wt % polyvinylidene fluoride (PVDF) on a nickel foam. Then the electrode was dried at 80 °C for 12 h under vacuum, and subsequently pressed at a pressure of 20 MPa. The loading mass of C/NiO nanosheet coated onto nickel foam was about 1.0 mg, and area was 1.0 cm². Cyclic voltammograms (CV), galvanostatic charge-discharge (GCD), and electrochemical impedance studies (EIS) were carried out on a CHI 660D electrochemical workstation. CV curves were collected in the potential range of 0.00–0.75 V vs. Ag/AgCl at varying the scan rate from 10 to 100 mV s⁻¹. GCD measurements were conducted at 5–25 A g⁻¹ in potential range of 0.00–1.00 V vs. Ag/AgCl. EIS measurements were obtained in the 0.01 Hz and 100 kHz at the open circuit voltage with an alternate current amplitude of 5 mV.

Results and discussion

The photographs of the precursor and the product after annealing process are shown in Figure S1. All the diffraction peaks of precursor (Figure S2a) can be assigned to XRD pattern of ZIF-8, which had been reported in the previous literature.³⁷ On the other hand, it can be clearly seen that the volume of annealed product was expanded for several times. As seen from the TGA curve (Figure S2b), Ni-ZIF-8 has an obvious weight loss from 175 to 300 °C, which can be ascribed to the collapse of the structure of MOFs and the evaporation (or thermal decomposition) of 2-methylimidazole.

Our experiment has taken a rapid heating method. Huge amounts of gas generated from the evaporation (or thermal decomposition) of the 2-methylimidazole play a role of pore former. Figure 1a and f show SEM images of the product after annealing process. It is observed that the foam-like products are constructed of plenty of interlinked nanosheets. The nanosheets have uniform thicknesses (less than 100 nm) and the surfaces are quite smooth. Figure 1b-e show elemental mapping of SEM images in Figure 1a denote the presence of carbon, nitrogen, nickel and oxygen elements, which are uniform distributed in the nanosheets. Figure 2a shows the XRD pattern of the nanosheet in a range from $2\theta = 20$ to 80° . The diffraction peaks around 37.2° , 43.3° , 62.9° and 75.4° can separately be assigned to (111), (200), (220) and (311) planes of crystallised cubic NiO phase (JCPDS 47-1049), and the intensive broad peak between 20° and 30° can be attributed to the nitrogen-doped carbon. Figure 2b shows TGA curve of C/NiO nanosheet from 100°C to 800°C with a ramp of 5°C min^{-1} . It is clearly to see that C/NiO nanosheet underwent significantly weight loss of 46.2% when heated to 400°C in air atmosphere. This weight loss can be ascribed to the combustion of carbon part. Correspondingly, the content of NiO in C/NiO nanosheet can be determined to 53.8%.

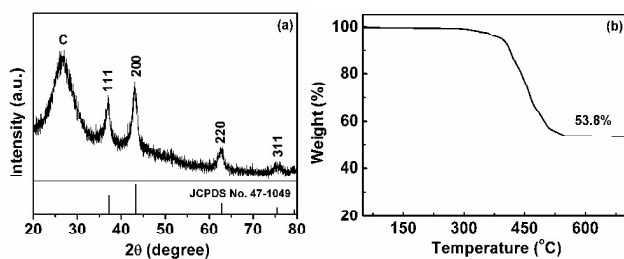


Fig. 2 (a) XRD pattern and (b) TG analysis of carbon/NiO nanosheet in air atmosphere.

Moreover, the structural features of C/NiO nanosheet were investigated by TEM and HRTEM (Figure 3a, b and c). In the sonication process of sample preparation, foam structure of products has been destroyed. The corresponding TEM images in Figure 3a and b clearly reveal that numerous nickel oxides nanoparticles are homogeneous distributed and embedded in the carbon nanosheet. The nanoparticles size of major nickel oxides is less than 10 nm (Figure 3b). Figure 3c shows a magnified HRTEM image of the nickel oxides nanoparticles. The lattice fringes with an interplanar spacings of 2.43 \AA are well corresponded to the lattice

fringe of the (111) crystal planes of NiO, which is also consistent with the $2\theta = 37.2^\circ$ peaks in the XRD pattern. It is worth noticing that there are pores and crevices between the nanoparticles. To further investigate the porosity of the C/NiO nanosheet, BET measurement is carried out. N_2 sorption isotherm of C/NiO nanosheet and corresponding pore size distribution is shown in Figure 3d. Through calculating, the specific surface area of C/NiO nanosheet is determined to be $138 \text{ m}^2 \text{ g}^{-1}$. The pore size distribution (Figure 3d inset) derived from N_2 adsorption shows an intensive peak at around 9 nm and a small half-peak in the range of less than 4 nm, which can be attributed to the particle size of NiO and the pores (or crevices) between them, respectively.

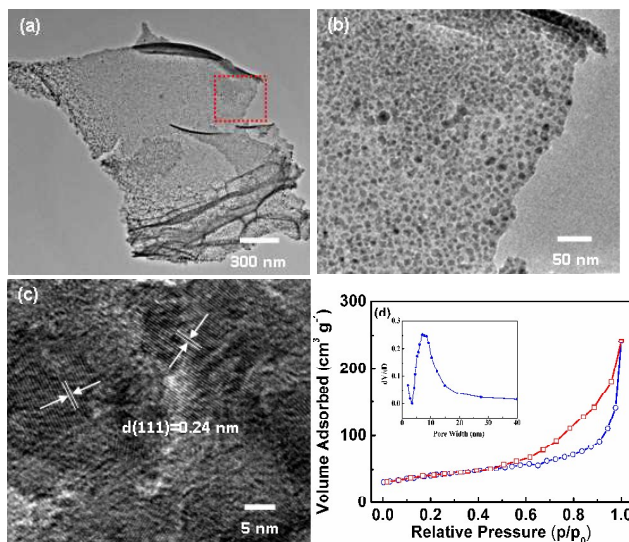


Fig. 3 (a,b) TEM and (c) HRTEM of the prepared C/NiO nanosheet. (d) N_2 sorption isotherms of C/NiO nanosheet with inset showing pore size distributions.

The elementary compositions of nanosheet were further analyzed through EDS. The EDS data in Figure 4a confirm that the nanosheet is composed of amorphous C, N, O and Ni elements (the Cu signal comes from the holey copper TEM grid). The results shows the C, N, O and Ni atomic ratio are 66.21% : 5.76% : 14.24% : 13.79%. Depending on EDS to calculate, the mass fraction of NiO embed in nanocomposite is 54.22%. This fraction is very close to the result of TG analysis.

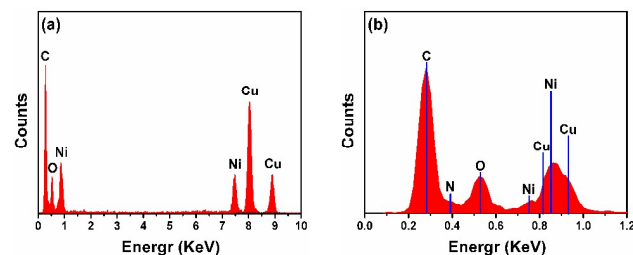


Fig. 4 (a,b) EDS images of the carbon/NiO nanosheet.

XPS is carried out to investigate the elemental composition and bonding configuration in the C/NiO nanosheet. The survey spectrum (Figure 5a) confirms the existence of carbon (C 1s), nitrogen (N 1s), oxygen (O 1s) and nickel (2p and 3p) elements in the sample. The C 1s XPS spectra spectrum (Figure 5b) can be fitted into three components: the sp²-hybridized carbon bond (sp² C-sp² C), sp²-hybridized C-N and sp³-hybridized C-N which are located at 284.7, 285.5 and 286.6 eV, respectively.³⁸ The XPS spectra of N 1s (Figure 5c) can be fixed into with two peaks at 398.5 and 400.6 eV for pyridinic N and pyrrolic N, respectively.^{39,40} The Ni 2p spectrum can be mainly fitted with the doublet of Ni²⁺ with a 2p_{3/2} binding energy of 229.7 eV and the doublet of Ni³⁺ at the lower energy (Figure 5d)^{41,42} The results can be certainly identified and further demonstrated the formation of the N-doped carbon, and the N/C atomic ratios in the C/NiO nanosheet are 11.34%, which are very agreement with the result of EDS. N-doped will offer abundant active site and reduce the polarization for electrochemical reaction, and thus improve the electrochemical performance of the material.

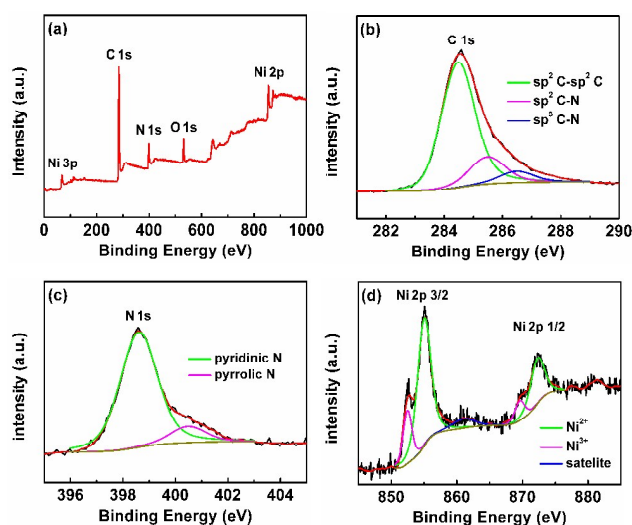
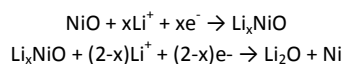


Fig. 5 XPS spectra of (a) survey spectrum, (b) C 1s, (c) N 1s, and (d) Ni 2p for C/NiO nanosheet.

The lithium store performance of the C/NiO nanosheet was investigated by CV. Figure 6a shows the CV curves of the C/NiO nanosheet in the first three cycles. During the first cathodic scanning, the C/NiO nanosheet electrode exhibits two reduction peaks at around 0.75 and 0.15 V, which can be mainly attributed to lithium intercalation into NiO nanoparticles along with the formation of surface electrolyte interphase (SEI) film and the reduction of Li_xNiO to Ni with the formation of Li₂O, respectively.⁴³ The related electrochemical reaction equations are believed to be as follows:



Because carbon content is high in the C/NiO nanosheet, the reduction peaks of NiO is covered up by the slope of Li⁺ intercalation on carbon and become not evidence. Identically, two oxidation peaks located at around 1.75 and 2.29 V can be observed

in the first anodic scanning, correspond to the Li⁺ deintercalation of carbon accompanying with partial decomposition of the SEI film and the oxidation of metallic Ni to form Li₂O, respectively.^{44,45} In the subsequent cycles, the lithium ion insertion/extraction reactions of the C/NiO nanosheet are similar and the electrochemical redox reactions become more reversible, involving that the reduction peak shift to 0.87 V and the oxidation peaks occurs at 1.87 and 2.29 V.

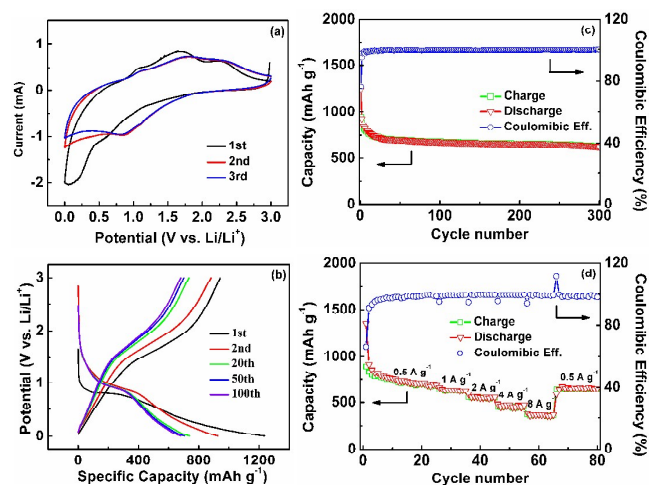


Fig. 6 Electrochemical lithium-storage performances of C/NiO nanosheet electrode: (a) CV curves for the first three cycles; (b) charge and discharge profiles for the 1st, 2nd, 20th, 50th and 100th cycles at a current density of 0.5 A g⁻¹; (c) cycling performance at a current density of 0.5 A g⁻¹ and (d) rate performance at various current densities.

Figure 6b shows the discharge and charge profiles of the C/NiO nanosheet for the 1st, 2nd, 20th, 50th and 100th cycles at a current density of 0.5 A g⁻¹. The first discharge and charge capacities of the C/NiO nanosheet electrode are 1236 and 942 mA h g⁻¹, respectively, accompanying with a coulombic efficiency of about 76.2%. The initial loss is mainly caused by the formation of SEI film and other irreversible reaction during the first cycle.⁴⁴ In the second cycle, the discharge capacity of the C/NiO nanosheet electrode is decreased to 926 mA h g⁻¹ followed by charge capacity of 882 mA h g⁻¹, giving rise to a high coulombic efficiency of about 95.2%. Subsequently, the discharge capacities are delivered about 735, 702, and 681 mA h g⁻¹ after 20, 50 and 100 cycles at a current rate of 0.5 A g⁻¹, respectively. Remarkably, a reversible capacity of 627 mA h g⁻¹ can be retained after 300 cycles, with coulombic efficiency very closed to 100% (Figure 6c). In addition, the structural features of monodisperse NiO embedded in carbon nanosheet can still be maintained after 300 cycles (Figure S3) although the NiO nanoparticles become a bit larger, suggested that the C/NiO nanosheet has outstanding lithium storage reversibility. The rate performance of the C/NiO nanosheet is evaluated at various current densities in a ranging from 0.5 to 8 A g⁻¹. As shown in Figure 6d, the C/NiO nanosheet electrode exhibits average reversible capacities of 690, 624, 550, 453, 360 mA h g⁻¹ at current densities of 0.5, 1, 2, 4 and 8 A g⁻¹, respectively. And when the current density is got back to 0.5 A g⁻¹ after 65 cycles, the reversible capacity of the C/NiO

nanosheet electrode rapid return to about 650 mAh g^{-1} , indicating the excellent LIBs rate performance. And the well performance of the assembled lithium ion batteries can be attributed to the unique structure of the mesoporous carbon/NiO nanosheet, which not only shortened the electro- and iron-transport path-ways but also accommodated the volume change during Li^+ intercalation and deintercalation process.

To investigate the supercapacitive performance, the as-prepared C/NiO nanosheet is measured in a three electrode system. Figure 7a shows the typical CV curves of C/NiO nanosheet electrode with different scan rates, ranging from 10 to 100 mV s^{-1} . As shown in the figure, all the CV curves have a pair of redox peaks, which represents pseudocapacitive behavior of the NiO nanoparticles in the C/NiO nanosheet.⁴⁶ In addition, the part of CV curves without redox peaks show quasi-rectangular shapes, which can be ascribed as the typical performance of electric double-layer capacitors (EDLCs) of the nitrogen-doped mesoporous carbon.^{47,48} All the above results demonstrate that the energy storage mechanism of the C/NiO nanosheet electrode mainly included faradaic redox reactions and electrostatic mechanism. Moreover, despite the slightly shift of redox peaks, the shape of the CV curves is not significantly changed at different scan rates ranged from 10 to 100 mV s^{-1} , indicating good electrochemical reversibility of the C/NiO nanosheet electrode.

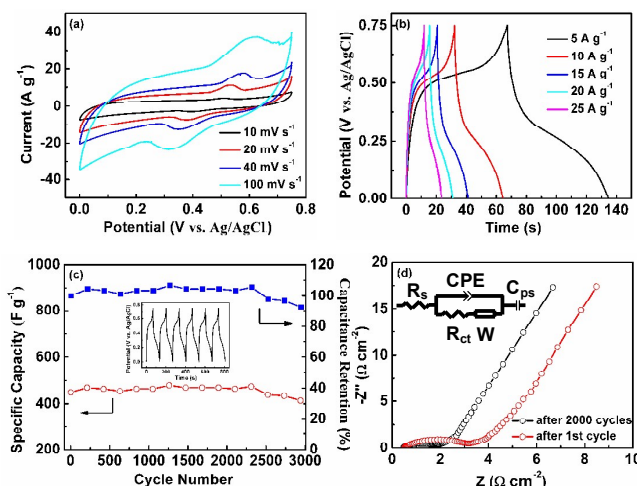


Fig. 7 Supercapacitive performances of the as-prepared C/NiO nanosheet electrode: (a) CV curves at various rates; (b) Charge and discharge curves at different current densities; (c) Cycling performance at a current density of 0.5 A g^{-1} with the corresponding capacitive retention. The inset shows the charge and discharge curves of the first five cycles; (d) Nyquist plots after the 1st and 2000th cycles.

The potential-time profiles of the C/NiO nanosheet at different current densities ranged from 5 to 25 A g^{-1} are shown in Figure 7b. The plateaus in each charge or discharge curves represent the redox reaction derived capacitance, which reveals pseudocapacitive behavior of the C/NiO nanosheet. It is matched well with the CV curves. The specific capacitance of the C/NiO nanosheet electrode is calculated from the following formula:

$$C = It / (\Delta Vm)$$

where C (F g^{-1}) is specific capacitance, I (A) represents the current density, Δt (s), ΔV (V) and m designate the discharge time, the voltage range and the mass of active materials, respectively. Therefore, the specific capacitance of NiO can be calculated up to 449 F g^{-1} at 5 A g^{-1} (Figure 5b). Even at 25 A g^{-1} , the specific capacitance is still as high as about 390 F g^{-1} , suggesting that the mass transportation and electron conduction was greatly improved by the special morphology of C/NiO nanosheet.

In addition, the supercapacitive stability of the C/NiO nanosheet electrode is further manifested by its ultralong cycle performance. Figure 7c shows the cycling performance of the C/NiO nanosheet electrode over 3000 cycles. The C/NiO nanosheet can deliver a specific capacitance of 414 F g^{-1} , (0.414 F cm^{-2}) at 5 A g^{-1} corresponding to a capacitance retention of 92.2% after 3000 cycles, that is undisputed higher than many previously reported carbon, NiO and their hybrid materials (see Supporting Information Table S1). This result proves that the nitrogen-doped mesoporous interlinked carbon embedded by NiO nanoparticles largely improves the rate capability and the cycle stability of two components.

Figure 7d displays the Nyquist plots of C/NiO nanosheet after 1 and 2000 cycles. The equivalent circuit (as shown in the inset of Figure 7d) is used to fitting the EIS experimental results, where R_s is the solution resistance, R_{ct} is the charge-transfer resistance, CPE is the interfacial capacitance and C_{ps} represents faradaic pseudocapacitance. The values of R_s and R_{ct} are determined to be 0.46 and 1.34Ω for C/NiO nanosheet supercapacitor after 2000 cycles, which are smaller than the initial resistance (0.50 and 2.66Ω). This is mainly because active materials had undergone an activation process as the test proceeds. The slopes of the impedance plots in low frequency represent diffusion impedance or Warburg element of the electrolytic ion in the solid phase electrode surface. As can be seen in the figure, there is almost no change of the slopes after 2000 cycles, suggesting the excellent cycling stability of the C/NiO nanosheet electrode.

Conclusions

A new nitrogen-doped mesoporous interlinked carbon/NiO nanosheet has been synthesized through very simple method. Based on the distribution of nickel metal ions in MOFs, the generated monodisperse NiO nanoparticles are homogeneously embedded in carbon nanosheet. The as-obtained carbon/NiO nanosheet has a specific surface area as high as $138 \text{ m}^2 \text{ g}^{-1}$. The unique mesoporous structure of the carbon/NiO nanosheet not only provides short transport path for electronic and ionic but also accommodates the volume change during electrochemical reaction. In addition, N-doped can offer abundant active site for the carbon/NiO nanosheet electrode, resulted in the electrochemical performance of it improved to a certain extent. Based on the mentioned merits, the carbon/NiO nanosheet exhibits excellent cycling stability (627 mAh g^{-1} after 300 cycles at 0.5 A g^{-1} for LIBs, and 414 F g^{-1} after 3000 cycles at 5 A g^{-1} for supercapacitor) and high rate performance (360 mAh g^{-1} at 8 A g^{-1} for LIBs, and 390 F g^{-1} at 25 A g^{-1} for supercapacitor) in both LIBs and supercapacitor. We believe our results will provide an impetus to exploit easy access to new structures and candidates for energy storage.

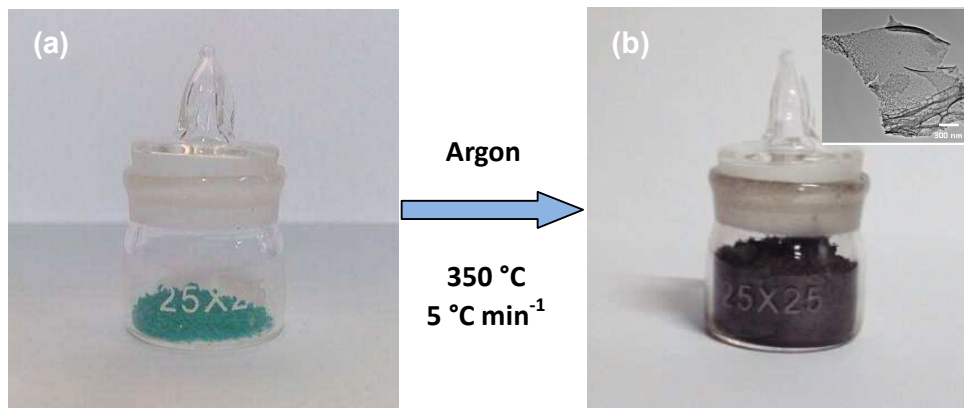
Acknowledgements

This work was supported by the financial supports of the National Natural Science Foundation of China (Nos. 21301140 and 21061130551), the Natural Science Foundation of Shaanxi Province (No. 2013JQ2004), and the Xi'an Industrial Technology Innovation Project-technology transfer promoting program (No. CXY1438-6).

References

- 1 X. P. Gao, H. X. Yang, *Energy Environ. Sci.*, 2010, **3**, 174.
- 2 M. V. Reddy, G. V. Subba Rao, B. V. R. Chowdari, *Chem. Rev.* 2013, **113**, 5364.
- 3 W. T. Hong, M. Risch, K. A. Stoerzinger, A. Grimaud, J. Suntivich, Y. Shao-Horn, *Energy Environ. Sci.*, 2015, **8**, 1404.
- 4 P. Roy, S. K. Srivastava, *J. Mater. Chem. A*, 2015, **3**, 2454.
- 5 M. Zhi, C. Xiang, J. Li, M. Li, N. Wu, *Nanoscale*, 2013, **5**, 72.
- 6 H. Kim, G. Jeong, Y. Kim, J. Kim, C. Park, H. Sohn, *Chem. Soc. Rev.*, 2013, **42**, 9011.
- 7 P. Roy, S. K. Srivastava, *J. Mater. Chem. A*, 2015, **3**, 2454.
- 8 J. Lin, J. L. Guo, C. Liu, H. Guo, *ACS Appl. Mater. Interfaces*, 2015, **7**, 17311.
- 9 F. Zou, X. Hu, Z. Li, L. Qie, C. Hu, R. Zeng, Y. Jiang, Y. Huang, *Adv. Mater.* 2014, **26**, 6622.
- 10 T. T. Chen, Y. Fan, G. G. Wang, Q. Yang, R. X. Yang, *RSC Adv.*, 2015, **5**, 74523.
- 11 M. Hou, K. Sun, X. L. Deng, F. L. Xiao, H. Yang, *RSC Adv.*, 2015, **5**, 74664.
- 12 L. Li, Z. Wu, S. Yuan, X. B. Zhang, *Energy Environ. Sci.*, 2014, **7**, 2101.
- 13 P. Roy, S. K. Srivastava, *J. Mater. Chem. A*, 2015, **3**, 2454.
- 14 H. Q. Li, H. S. Zhou, *Chem. Commun.*, 2012, **48**, 1201.
- 15 X. H. Xia, Y. Q. Zhang, D. L. Chao, C. Guan, Y. J. Zhang, L. Li, X. Ge, I. M. Bacho, J. P. Tu, H. J. Fan, *Nanoscale*, 2014, **6**, 5008.
- 16 Bin Liu, Jun Zhang, Xianfu Wang, Gui Chen, Di Chen, Chongwu Zhou, and Guozhen Shen, *Nano Lett.*, 2012, **12**, 3005.
- 17 X. L. Wang, G. Q. Shi, *Energy Environ. Sci.*, 2015, **8**, 790.
- 18 G. M. Zhou, F. Li, H. M. Cheng, *Energy Environ. Sci.*, 2014, **7**, 1307.
- 19 J. G. Kim, Y. Kim, Y. Noh, W. B. Kim, *RSC Adv.*, 2014, **4**, 27714.
- 20 S. Yuvaraj, S. Amaresh, Y. S. Lee, R. K. Selvan, *RSC Adv.*, 2014, **4**, 6407.
- 21 Y. Y. Shen, *J. Mater. Chem. A*, 2015, **3**, 13114.
- 22 X. Jiang, X. L. Yang, Y. H. Zhu, Y. F. Yao, P. Zhao, C. Z. Li, *J. Mater. Chem. A*, 2015, **3**, 2361.
- 23 H. Q. Li, H. S. Zhou, *Chem. Commun.*, 2012, **48**, 1201.
- 24 J. A. Mason, M. Veenstra, J. R. Long, *Chem. Sci.*, 2014, **5**, 32.
- 25 L. J. Murray, M. Dinca, J. R. Long, *Chem. Soc. Rev.*, 2009, **38**, 1294.
- 26 J. A. Mason, K. Sumida, Z. R. Herm, R. Krishna, J. R. Long, *Energy Environ. Sci.*, 2011, **4**, 3030.
- 27 G. Huang, F. F. Zhang, L. L. Zhang, X. C. Du, J. W. Wang, L. M. Wang, *J. Mater. Chem. A*, 2014, **2**, 8048.
- 28 R. B. Wu, X. K. Qian, X. H. Rui, H. Liu, B. L. Yadian, K. Zhou, J. Wei, Q. Y. Yan, X. Q. Feng, Y. Long, L. Y. Wang, Y. Z. Huang, *small*, 2014, **10**, 1932.
- 29 T. Yi Ma, L. Liu, Z. Y. Yuan, *Chem. Soc. Rev.*, 2013, **42**, 3977.
- 30 Z. X. Wu, P. A. Webley, D. Y. Zhao, *J. Mater. Chem.*, 2012, **22**, 11379.
- 31 Y. H. Su, H. L. Jiang, Y. H. Zhu, X. L. Yang, J. H. Shen, W. J. Zou, J. D. Chen, C. Z. Li, *J. Mater. Chem. A*, 2014, **2**, 7281.
- 32 J. P. Paraknowitsch, A. Thomas, *Energy Environ. Sci.*, 2013, **6**, 283.
- 33 H. J. Lu, Y. Li, L. Q. Zhang, H. N. Li, Z. X. Zhou, An. R. Liu, Y. J. Zhang, S. Q. Liu, *RSC Adv.*, 2015, **5**, 52126.
- 34 X. T. Qing, Y. Cao, J. Wang, J. J. Chen, Y. Lu, *RSC Adv.*, 2014, **4**, 55971.
- 35 P. Wu, Y. D. Qian, P. Du, H. Zhang, C. X. Cai, *J. Mater. Chem.*, 2012, **22**, 6402.
- 36 L. Zhou, H. Cao, S. Q. Zhu, L. R. Hou and C. Z. Yuan, *Green Chem.*, 2015, **17**, 2373.
- 37 J. F. Yao, H. T. Wang, *Chem. Soc. Rev.*, 2014, **43**, 4470.
- 38 L. Perini, C. Durante, M. Favaro, V. Perazzolo, S. Agnoli, O. Schneider, G. Granozzi, A. Gennaro, *ACS Appl. Mater. Interfaces*, 2015, **7**, 1170.
- 39 W. J. Yuan, J. C. Li, L. K. Wang, P. Chen, A. J. Xie, Y. H. Shen, *ACS Appl. Mater. Interfaces*, 2014, **6**, 21978.
- 40 K. J. Zhang, L. X. Zhang, X. Chen, X. He, X. G. Wang, S. M. Dong, L. Gu, Z. H. Liu, C. S. Huang, G. L. Cui, *ACS Appl. Mater. Interfaces*, 2013, **5**, 3677.
- 41 S. J. Feng, W. Yang, Z. B. Wang, *Materials Science and Engineering B*, 2011, **176**, 1509.
- 42 Md. E. Uddin, N. H. Kim, T. Kuila, S. Hee Lee, D. Hui, J. H. Lee, *Composites Part B*, 2015, **79**, 649.
- 43 H. Wu, M. Xu, H. Y. Wu, J. J. Xu, Y. L. Wang, Z. Peng, G. F. Zheng, *J. Mater. Chem.*, 2012, **22**, 19821.
- 44 S. H. Park, W. J. Lee, *RSC Adv.*, 2015, **5**, 23548.
- 45 Y. Q. Zhu, H. Z. Guo, Y. Wu, C. B. Cao, S. Tao, Z. Y. Wu, *J. Mater. Chem. A*, 2014, **2**, 7904.
- 46 M. Khairy, S. A. El-Safty, *RSC Adv.*, 2013, **3**, 23801.
- 47 W. J. Zhou, K. Zhou, X. J. Liu, R. Z. Hu, H. Liu, S. W. Chen, *J. Mater. Chem. A*, 2014, **2**, 7250.
- 48 P. Hao, Z. H. Zhao, J. Tian, H. D. Li, Y. H. Sang, G. W. Yu, H. Q. Cai, H. Liu, C. P. Wong, A. Umar, *Nanoscale*, 2014, **6**, 12120.
- 49 J. H. Hou, C. B. Cao, F. Idrees, X. L. Ma, *ACS nano.*, 2015, **9**, 2556.
- 50 R. Carter, L. Oakes, A. P. Cohn, J. Holzgrafe, H. F. Zarick, S. Chatterjee, R. Bardhan, C. L. Pint, *J. Phys. Chem. C*, 2014, **118**, 20137.
- 51 Y. H. Li, H. R. Peng, C. Zhang, M. S. Chu, P. Xiao, Y. H. Zhang, *RSC Adv.*, 2015, **5**, 77115.
- 52 W. J. Ji, J. Y. Ji, X. H. Cui, J. J. Chen, D. J. Liu, H. Deng, Q. Fu, *Chem. Commun.*, 2015, **51**, 7669.
- 53 Y. G. Zhu, G. S. Cao, C. Y. Sun, J. Xie, S. Y. Liu, T. J. Zhu, X. B. Zhao, H. Y. Yang, *RSC Adv.*, 2013, **3**, 19409.
- 54 B. Zhao, J. S. Song, P. Liu, W. W. Xu, T. Fang, Z. Jiao, H. J. Zhang, Y. Jiang, *J. Mater. Chem.*, 2011, **21**, 18792.
- 55 S. P. Jahromi, A. Pandikumar, B. T. Goh, Y. S. Lim, W. J. Basirun, H. N. Lim, N. M. Huang, *RSC Adv.*, 2015, **5**, 14010.
- 56 G. Cheng, Y. N. Yan, R. Chen, *New J. Chem.*, 2015, **39**, 676.
- 57 C. Z. Yuan, B. Gao, L. H. Su, X. G. Zhang, *Solid State Ionics*, 2008, **178**, 1859.
- 58 C. Z. Yuan, S. L. Xiong, X. G. Zhang, L. F. Shen, F. Zhang, B. Gao, L. H. Su, *Nano Research*, 2009, **2**, 722.

Graphical Abstract:



The precursor Ni-ZIF-8 and (b) the product after annealing process.

We report on a novel nitrogen-doped mesoporous interlinked carbon/NiO nanosheet fabricated using Ni-MOF-8 as both the precursor and the self-sacrificing template. The synthesis route includes a precipitation reaction to form MOFs at room temperature and a subsequently thermal treatment process at 350 °C in the argon protection. Our strategy is simple in operation and low in cost, and most important it is very applicable to large-scale production with good controllability. In the synthesized carbon/NiO nanosheet product, monodispersed NiO nanoparticles with an average particle size of around 10 nm are uniformly dispersed and embedded in mesoporous carbon. When evaluated as electrode materials, the as-prepared carbon/NiO nanosheet can exhibit high lithium storage capacity and excellent supercapacitive performance.